Second-order Raman spectroscopic study of lithium hydride and lithium deuteride at high pressure

Allen C. Ho* and Roland C. Hanson†
Department of Physics and Astronomy, Arizona State University, Tempe, Arizona 85287-1504

Andrew Chizmeshya
Materials Research Group, Arizona State University, Tempe, Arizona 85287-1604
(Received 13 February 1997)

Second-order Raman spectra of LiH and LiD have been measured as functions of pressure up to 15 GPa ($\Delta V/V_0 = -0.25$) at ambient temperature. The assignments of the many features in these spectra have been thoroughly studied. The features have been compared with the two-phonon dispersion curves derived from neutron-scattering data and with isotope effect scaling. In addition, an internal self-consistency procedure is employed to validate the phonon assignments. Most of the features are assigned to combinations of zone-boundary phonons. The pressure and volume dependence of many zone-boundary phonons have been determined. These include all of the phonons at the X point as well as some at the L and the W points. Most of these phonons have constant mode Grüneisen parameters, while others exhibit volume-dependent mode Grüneisen parameters. There is significant variation in the magnitude of these parameters between the various modes. The results are shown to be in good agreement with our *ab initio* calculations. [S0163-1829(97)00322-6]

I. INTRODUCTION

Lithium hydride and lithium deuteride are rocksalt-structure quantum crystals that are ideal candidates for both experimental and theoretical studies. There are only four electrons per unit cell, making them the simplest ionic crystals in terms of electronic structure. Moreover, there is a large isotope effect provided by proton and deuteron exchange. Because of these factors and because of their use in thermonuclear weapons, LiH and LiD have been extensively studied both theoretically and experimentally for the past four decades. An extensive review has recently been published by Islam.[1]

Second-order Raman scattering at high pressure offers a very attractive method for investigating phonon properties of crystals. The second-order Raman spectra reflect the two-phonon density of states, which can be compared directly with current lattice-dynamical theories. In the past, second-order Raman scattering at high pressure has been limited to semiconductor materials.[2] In this paper, we present the results of study[3] of the pressure dependence of the second-order Raman spectra of LiH and LiD.

The second-order Raman spectra of LiH and LiD have been studied by a number of groups. Jaswal *et al.*[4,5] made detailed measurements and a theoretical calculation of the second-order Raman spectra. They obtained complete spectra for all three group-theoretical symmetries. No attempt was made to assign the various features in the spectrum to critical points in the second-order density of states. They developed a deformation dipole model based on the neutron-scattering data[6] which explained many of the features in the spectra. Laplaze[7,8] studied the second-order Raman spectra of LiH and LiD and assigned the various features in the spectra to critical points based on the shell-model fits to neutron-scattering data.[6] Anderson and Lüty[9] subsequently made careful measurements on crystals of ^{6}LiH, ^{7}LiH, and ^{7}LiD. Using a simple force-constant model applied to zone-boundary phonons, they were able to classify the various features in the spectrum. By comparing with the data from the shell-model fit,[6] they assigned most of the features in the Raman spectra to zone-boundary phonons at the X and L points. Tyutyunnik and Tyutyunnik[10] studied the second-order Raman spectra of ^{6}LiH and ^{7}LiH. They showed that the features in the 2LO region of the spectrum exhibit a very strong resonance as the excitation wavelength is tuned to the ultraviolet. They used a similar force-constant model to the one used by Anderson and Lüty, but because they considered other high-symmetry points in addition to the X and L points they arrived at different assignments. More recently, Plekhanov and co-workers[11–18] have investigated the second-order Raman spectra at room temperature for mixed LiH_xD_{1-x} ($0 \leqslant x \leqslant 1$) crystals. These authors attributed the strong resonant component in the 2LO features to the 2LO (Γ) phonon. It should be noted that there is some mutual agreement between these attempts[7–10] to assign the various features, but there are also some significant differences.

In this paper, we report studies of the pressure dependence of the second-order Raman spectra of LiH and LiD at high pressure. We were motivated to attempt a Raman study of LiH and LiD using modern diamond-anvil-cell technology by the following reasons. First of all, the second-order Raman spectra of these crystals are unusually strong, making them suitable for Raman study in diamond-anvil cell. Second, in spite of a comprehensive collection of second-order Raman spectra, the assignment of various features in the second-order Raman spectra to critical points in the two-phonon density of states is still unclear. We will show that a study of the effects of pressure can remove some of these ambiguities. Third, the equation-of-state (EOS) measured by Besson *et al.*[19] will allow us to determine the mode Grüneisen parameters for a number of phonons at high-symmetry

zone-boundary points. Because of the large compressibility of the crystals we will be able to produce a large volume change with application of modest pressure; this will lead to mode Grüneisen parameters that are volume dependent. In a companion paper[20] we will compare our experimental results with *ab initio* calculations.

II. EXPERIMENT

Single crystals of LiH and LiD were furnished by the Crystal Growth Laboratory at the University of Utah. Special precautions were taken in handling these crystals since they are hygroscopic. A single crystal was loaded in a diamond-anvil cell with argon as the pressure-transmitting medium. The pressure was determined *in situ* by the calibrated shift in the ruby R_1 fluorescence line.[21]

High-pressure micro-Raman experiments were performed in a 135° backscattering geometry up to 15 GPa at ambient temperature. The experiments terminated at about 15 GPa because the quality of the spectra degraded. Raman measurements were also repeated at ambient pressure and temperature. Raman spectra were excited by the 5145 Å lines of an argon-ion laser. Other lines from the argon-ion laser and a krypton-ion laser extending to 4067 Å were also used in an attempt to observe the resonant Raman scattering described by earlier studies;[10,15,22,23] however the increased diamond luminescence prevented observations at these other wavelengths. The scattered light was dispersed by a triple spectrometer (Spex, Model 1877) using a 600 grooves/mm grating in the final dispersing stage. A liquid-nitrogen-cooled intensified charge-coupled device (Spex Spectrum One) was used for multichannel photon detection. A wide slit width was used, resulting in a resolution approximately equal to 10 cm^{-1}. This resolution is more than adequate considering the broad nature of the second-order Raman spectra that we are studying. All spectra were carefully calibrated by neon lines.

III. RESULTS

The second-order Raman spectra of LiD and LiH at several pressures are shown in Figs. 1(a) and 1(b), respectively. These Raman spectra taken on microscopic crystals in the diamond-anvil cell are of comparable quality to the earlier Raman spectra taken at ambient pressure and temperature on macroscopic crystals. The major resolved features are labeled following the conventions used in Refs. 9 and 10. However since we identify more features than previous authors did, letters are appended to numerals for subfeatures which were not explicitly identified previously or which became evident with increased pressure.

The main focus in this paper is on the pressure dependence of the frequencies of two-phonon features which are interpreted as critical points in the two-phonon density of states. There are few changes in the intensity of the various features, however some features take on the familiar characteristic appearance of critical points at high pressure. The detailed phonon assignment of these features will be deferred to a later section. For clarity these features will be labeled with the assignments that we will make later.

As shown in Figs. 1(a) and 1(b), the second-order Raman spectra of LiH and LiD are very rich in features. The pressure-dependent features in the second-order Raman spectra will now be discussed.

Features $1A-1E$ are identified as optic minus acoustic difference modes since they vanish at low temperature.[4,5,8,9] Feature $1A$ corresponds to the strong feature 1 seen in the earlier works. Higher-frequency features $1B$ and $1C$ are seen more clearly only in LiD as the pressure increases. We also observed the lower frequency difference features, $1D$ and $1E$, in LiH in our high-pressure spectra.

Features 2–5 are acoustic sum modes. In LiD features $2A$ and $2B$ become very evident at high pressure. Feature $2C$, which was seen as a sharp peak, feature 2 (Refs. 9 and 10) evolves into a square-root P_2 singularity at high pressure. The overlap between regions corresponding to feature 1 and feature 2 in the LiH spectra conceals many of the subfeatures seen in LiD. In LiH we were able to follow feature $2C$ as well as a new feature $2D$ which appeared weakly in a few spectra. In LiD features 3 and 4 become increasingly overlapped as pressure increases, while in LiH this does not occur. Feature 5 is clearly seen in both LiH and LiD.

Features $6-8C$ are acoustic plus optic sum modes. Features 6, 7, and $8A$ [feature 8 (Refs. 9 and 10)] are clearly seen in both LiH and LiD. Features $8B$ and $8C$ have been observed in LiD and LiH at ambient conditions by Plekhanov and co-workers.[11–18] Anderson and Lüty[9] observed feature $8C$ as a weak shoulder in their ^{6}LiH and ^{7}LiH Raman spectra at 300 K, however they labeled it as feature 9 in their figure. We will show later why we differentiate between $8B$ in LiD and $8C$ in LiH.

The optic sum mode region includes the previously identified features 9–12 (Ref. 9).[24] Feature 9 was previously observed only in LiH both at low temperature[9] and at ambient temperature.[10] We observed a weak indication of feature 9 in our LiH spectra, however it could not be reliably followed due to the background. Feature 9 was not observed in LiD. Feature 10 is a broad feature without apparent subfeatures, although Tyutyunnik and Tyutyunnik[10] saw two distinct features in this region. Feature 11 is resolved into features $11A$ and $11B$ which will be assigned to 2LO (X) and 2LO (L). The upper end of feature 11 will be called feature $11C$ and will correspond to 2LO (Γ). We *estimated* the location of $11C$ in LiD in all our spectra. In LiH all of feature 11 is in the same region as the second-order Raman spectrum of the diamond. We were unable to separate these two spectral contributions in order to locate subfeatures. Feature 12 in LiD is identified as the overtone of an impurity local mode involving H^- motion.[25]

Most of the data at ambient pressure used in the analysis come from Raman measurements that we repeated at ambient pressure and temperature. However, we have also used data from other sources to supplement our own. The frequencies at ambient pressure and temperature for features $8B$ and $8C$ in LiD and LiH, respectively, were read from the figures published by Plekhanov.[15] The ambient pressure data for feature 12 [$2\nu(H^-)$] was measured by Plekhanov and Veltri.[11,12]

The pressure dependence of the frequencies of the various second-order features plotted as a function of pressure for

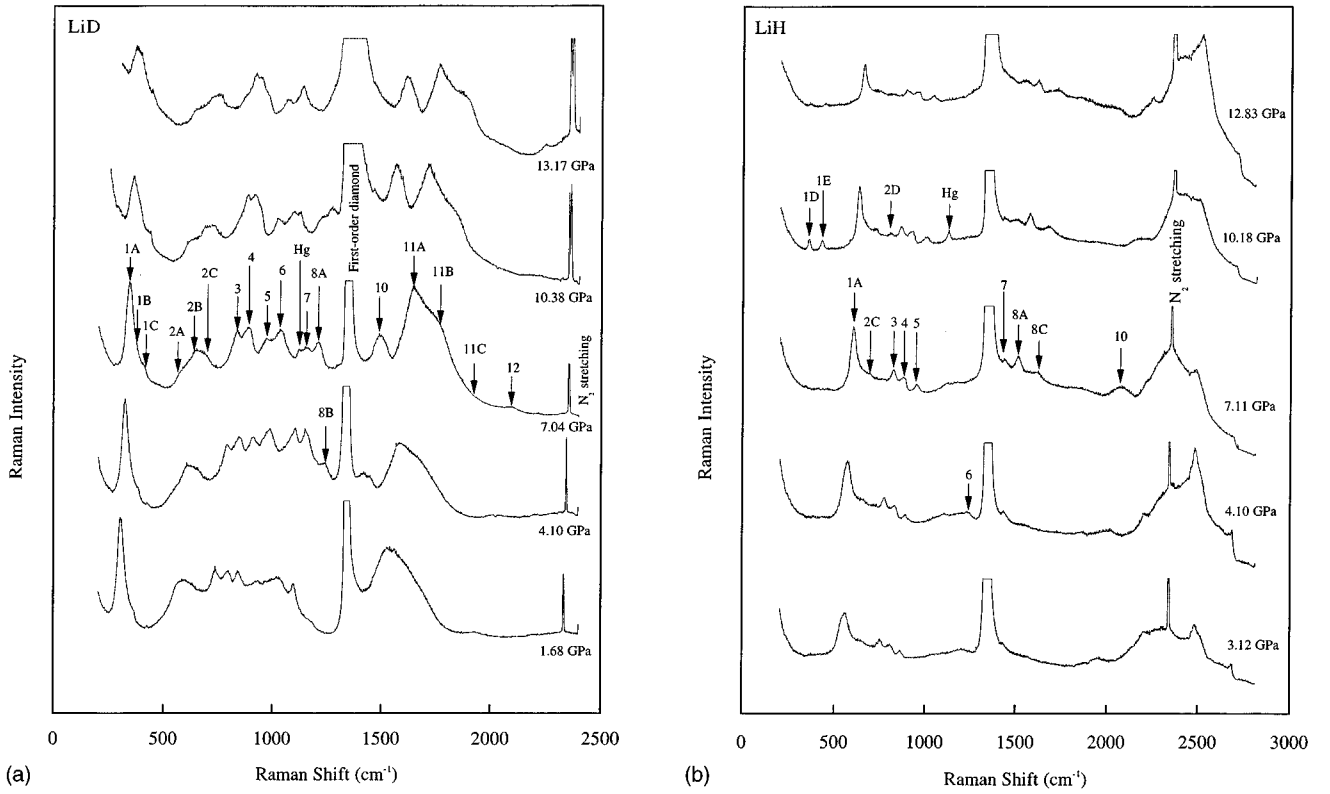

FIG. 1. The second-order Raman spectra of LiD and LiH at high pressure. (a) LiD, (b) LiH. All spectra were taken at room temperature. The major resolved features are labeled and followed as functions of pressure. The intense peak in the middle is the first-order Raman peak of the diamond, which prohibits direct observation of features when they move into it. Features $1A-C$ are optic minus acoustic difference modes. Features 2–5 are acoustic sum modes. Features 6–8 are acoustic plus optic sum modes. Features $10-11C$ are optic sum modes. Feature 12 is the overtone of the H^- impurity mode in LiD. Feature 11 in LiH was obscured by the second-order Raman spectrum of the diamond.

both LiH and LiD are shown in Figs. 2–5. These features are classified into the following four groups: acoustic sum modes in Fig. 2; optic sum modes in Fig. 3; acoustic plus optic sum modes in Fig. 4; and optic minus acoustic difference modes in Fig. 5. The various frequencies have been fit to second-order polynomials in pressure. The coefficients of these fits are given in the Ref. 3.

IV. ANALYSIS OF ASSIGNMENTS

A. Two-phonon dispersion curves and density of states

As we have mentioned above, several of the earlier studies[7–10] have made attempts at assigning these features, mostly based on a comparison with the shell-model fit to the neutron-scattering data.[6] We shall also use this model as a starting point in our analysis. The assignments made in the previous studies are summarized in Table I. In the same table the current assignments are also given. We have used the shell model with the parameters determined by Verble, Warren, and Yarnell[6] to calculate the phonon frequencies. The frequencies are used to generate the two-phonon dispersion curves and the two-phonon density of states at ambient pressure and temperature which are shown in Fig. 6. This model produces a two-phonon density of states that is in qualitative agreement with the second-order Raman spectra. The results for LiH are similar, except that the optic branches are much higher in frequency than the acoustic branches and the optic-acoustic difference and acoustic sum branches overlap. Comparing the two-phonon dispersion curves and the two-phonon density of states with the experimental Raman spectra reveals a number of possible assignments of the observed features. This comparison is an essential part of our analysis.

Features $2A$, $2B$, $2C$, $2D$, 3, 4, and 5 are acoustic sum modes. In the present work feature 2 in LiD shows much substructure. The higher frequency feature $2C$ must be 2TA (X) by comparison with Fig. 6, while the lower frequency $2B$ must correspond to 2TA (L). Features $2A$ and $2D$ are likely to be due to interior points in the Brillouin zone. Feature 3 has been variously assigned. We will show later that the TA+LA (X) assignment is unambiguous. Feature 4 has presented something of a problem. In the two-phonon density of states from the shell model at ambient pressure feature 3 and feature 4 are not resolved. In our companion theoretical paper this problem will be resolved by showing that feature 4 can be unambiguously assigned as $2A_2$ (W).[26] Feature 5 has almost always been assigned as 2LA (X). The dispersion curves agree with this assignment, but also reveal that there may be a contribution from TA+TO (L).

Features 10 and $11A-C$ are optic sum modes. Feature 10 has been previously assigned as TO+LO (X,L,Γ). It is obvious by looking at the two-phonon dispersion curves that there is a broad region in the Brillouin-zone where the frequency of these sum modes are nearly constant. While the calculated second-order density of states clearly indicates the presence of two features in this region, we observe only one overall feature. Our assignment corresponds to these earlier

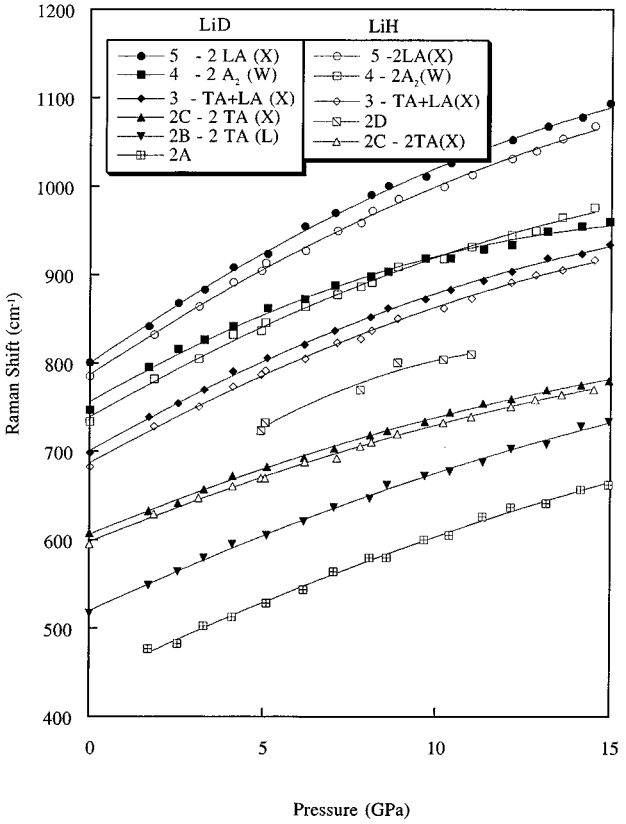

FIG. 2. The pressure dependence of the acoustic sum modes, features 2–5, for LiH (open symbols) and LiD (closed symbols). The curves are quadratic fits.

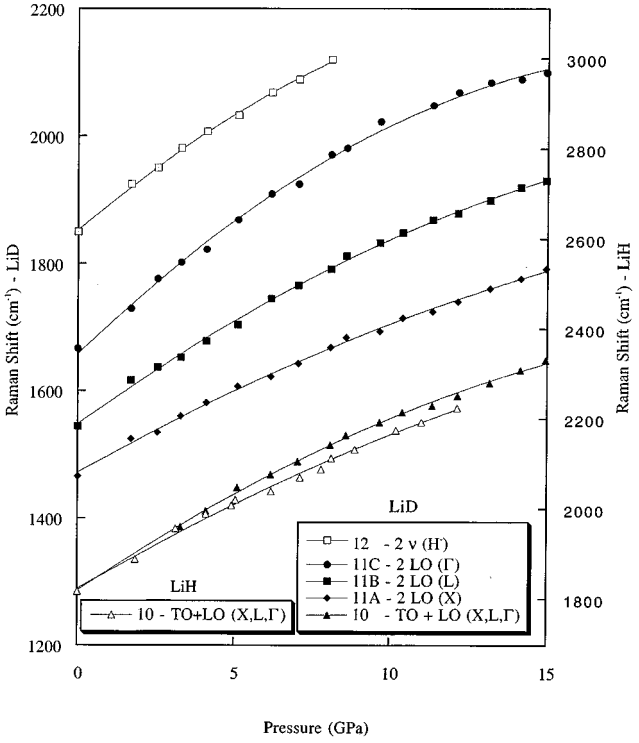

FIG. 3. The pressure dependence of the optic sum modes, feature 10 for LiH (open symbols) and features 10, 11*A*, *B*, *C*, and 12 for LiD (closed symbols). The LiH features are scaled by $\sqrt{2}$ relative to LiD features since these features are due mostly to hydrogen motion. Feature 10 agrees with this scaling. Feature 11*C* is our estimate of 2LO (Γ). Feature 12 in LiD is the overtone of the H^- impurity mode. The curves are quadratic fits.

assignments. Feature 11 corresponds to the 2LO region. In the earlier studies some authors[7,9] have realized that there are two separate component in this feature. In LiD the singularities 11*A* and 11*B* develop very clearly at high pressure. By comparing with Fig. 6, these can only be assigned as 2LO (*X*) and 2LO (*L*). The end of the spectrum is labeled 11*C*. Although this is not a clear singularity, comparison with Fig. 6 indicates that this is 2LO (Γ). Because of its importance we have *estimated* its location. A more complete discussion and comparison between the shape of the observed features and the expected Van Hove singularities deduced from the shell-model fit to neutron-scattering data is given in Ref. 3

B. Isotope effects

A simple force-constant model was used in early studies[9,10] to classify the effect of isotope substitution on the various features in the second-order Raman spectra, and thus to put constraints on the assignments of the various features. The model that has been used relies on two assumptions: The first is that for zone-boundary acoustic phonons only the heavier Li^+ ions move, while for zone-boundary optic phonons the lighter H^- or D^- ions move. This is strictly true only for zone-boundary phonons along certain high-symmetry directions, i.e., the *X* and *L* points in the Brillouin zone. The second assumption is that for a simple model of lattice dynamics that can be represented by harmonic springs between nearest-neighbor ions, the same force constant can be used for both acoustic and optic modes. Using these assumptions and the various isotope masses, Anderson and Lüty were able to classify all the modes in the second-order Raman spectra into five classes. These classes are (*A*) optic sum modes with only H^- or D^- ion motion; (*B*) acoustic sum modes with only Li^+ ion motion; (*C*) reduced-mass motion at the zone center; (*D*) mixed difference modes, optic minus acoustic; and (*E*) mixed sum modes, acoustic plus optic. Note that the letters assigned for these classes in Ref. 9 have no relation to the letters we have used to designate subfeatures in the spectra.

The frequency ratios between LiH and LiD for these various classes will now be discussed. Class *A* modes involve modes that both involve mainly H^- or D^- ion motion, so that the frequencies should scale by $\sqrt{2}$ between LiH and LiD. Class *B* modes involve mainly Li^+ ion motion, so they should have the same frequency for both LiH and LiD. Class *C* modes involving zone-center optic modes should scale by the square root of the reduced mass. The frequency ratios for class *D* and *E* are slightly more complicated. The relation between the two frequencies for *D* and *E* are given by

$$\frac{\nu_{\mathrm{LiH}}}{\nu_{\mathrm{LiD}}}=\frac{(\omega_1^0\mp\omega_2^A)_{\mathrm{LiH}}}{(\omega_1^0\mp\omega_2^A)_{\mathrm{LiD}}}=\frac{\sqrt{2k_1^0/m_{\mathrm{H}}}\mp\sqrt{2k_2^A/m_{\mathrm{Li}}}}{\sqrt{2k_1^0/m_{\mathrm{D}}}\mp\sqrt{2k_2^A/m_{\mathrm{Li}}}}$$
$$=\begin{cases}1.891 & \text{for a type } D \text{ difference mode}\\ 1.269 & \text{for a type } E \text{ sum mode.}\end{cases} \quad (1)$$

Here, because both masses are involved, the ratios will

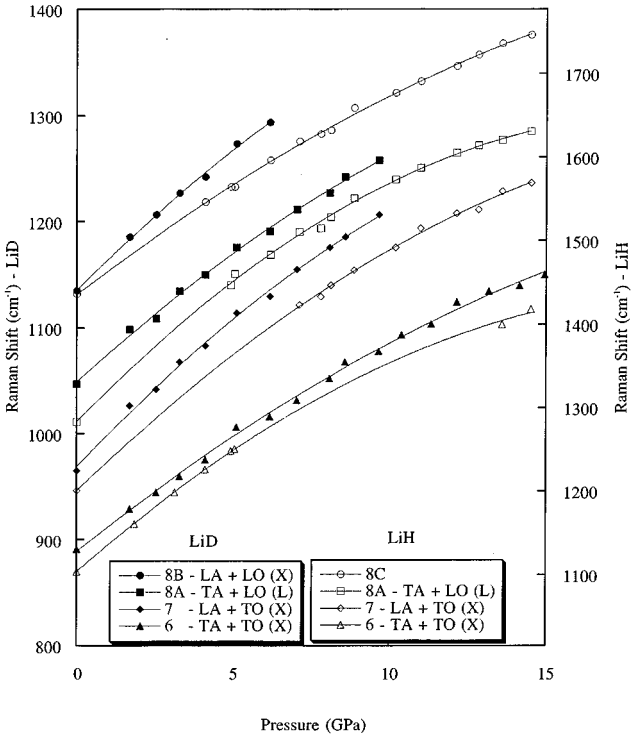

FIG. 4. The pressure dependence of the acoustic plus optic sum modes, features 6–8, for LiH (open symbols) and LiD (closed symbols). The LiH and LiD features are scaled by the ratio of 1.269:1. The curves are quadratic fits. See text.

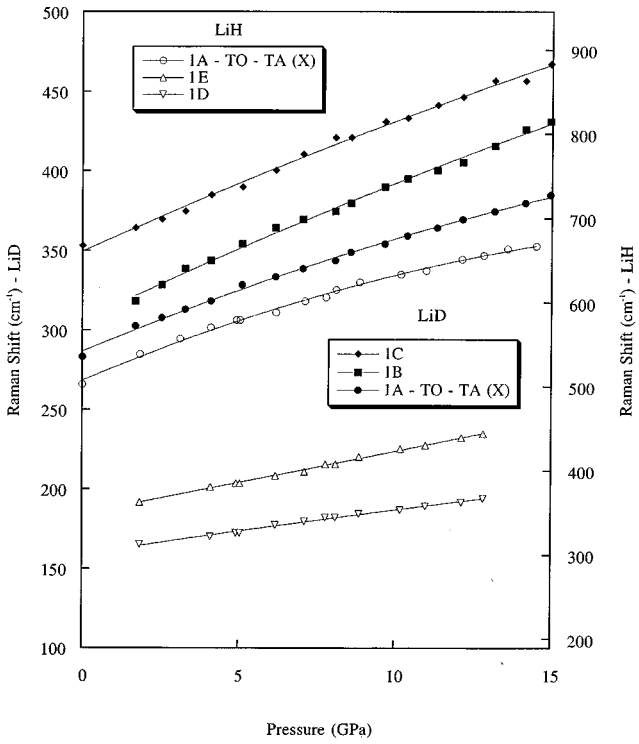

FIG. 5. The pressure dependence of the optic minus acoustic difference modes, features 1*A*, 1*D*, and 1*E*, for LiH (open symbols) and features 1*A*, 1*B*, and 1*C* for LiD (closed symbols). The LiH and LiD features are scaled by the ratio of 1.891:1. The curves are quadratic fits.

hold only if both force constants are the same. This will hold for combination modes involving either both transverse or both longitudinal modes. The expected ratio will not hold for transverse plus longitudinal combination modes. Thus, there may be class *D* and *E* combination modes that obey these expected ratios better than others. We will call the modes that obey the above scaling class D^* and class E^*.

In Fig. 2 the pressure dependence of features 2–5, the acoustic sum modes, class *B*, are plotted for both LiH and LiD using the same frequency scale. As can be seen, most of these features are nearly the same for LiH and LiD. In general the LiH frequencies are all slightly lower than their LiD counterparts; this is attributed to a slight softening of the force constant in LiH due to the larger zero point motion of the H^- ion. As we have mentioned earlier, feature 4 is anomalous for LiD since at higher pressures the LiD frequency crosses over to fall below the LiH frequency.

The optic sum modes, class *A*, feature 10 for LiH and features 10, 11*A*, 11*B*, and 11*C* for LiD, are shown in Fig. 3 with the $\sqrt{2}$ factor used for the LiH features. Feature 10 compares very favorably between LiH and LiD.

The acoustic plus optic sum mode, class *E* (features 6, 7, 8*A*, 8*B*, and 8*C*) are shown in Fig. 4. They are plotted with the LiD frequency on the left and the LiH frequency scaled by 1.269 [Eq. (1)] on the right. Feature 6 appears to scale with this ratio and is a class E^*. We will assign feature 6 to TA+TO (*X*). Features 7 and 8*A* scale less satisfactorily; they will be assigned to LA+TO (*X*) and TA+LO (*L*), respectively. Features 8*B* in LiD and 8*C* in LiH scale at ambient pressure, indicating that they may be the same feature; however the scaled frequencies of these two features move apart as the pressure increases.

The frequencies of the difference modes, class *D*, with the frequencies scaled by the 1.891 [Eq. (1)] factor are presented by Fig. 5. Only feature 1*A* can be compared between LiH and LiD. The 1*A* difference mode scales closely to this ratio indicating it is class D^*. This is consistent with the assignment of TO-TA (*X*).

C. Assignment by self-consistency

It was pointed out by Brafman and Mitra[27] that pressure studies may be used to clarify phonon assignment of multiphonon Raman spectra. In this earlier work, the authors applied this principle to identify the overtone and difference modes in a limited way. Here we will exploit this principle fully and demonstrate the utility of pressure dependence in phonon assignment.

We have verified assignments by the use of pressure-dependent self-consistency checks whenever possible. The procedure is described as follows. First, we assign the overtone features using the results from the shell-model fit to the neutron-scattering data; the overtone features in general can be assigned unambiguously. We also make trial assignments to other acoustic and optic sum features. These features are assigned with less confidence than the overtone features. These hypothetical assignments are tested by comparing the frequencies of the acoustic and optic sum features with combinations of individual phonon frequencies determined from the overtone features. The pressure dependence of all these features allow us to confirm or reject assignments that have

TABLE I. Assignments of features in the second-order Raman spectra of LiH and LiD showing previous proposals along with our assignments.

Feature	Laplaze[a]	Anderson and Lüty[b]	Tyutyunnik and Tyutyunnik[c]	Present work
1*A*	LA-TA (*L*)	TO-TA (*L*)	TO-TA (*W*,*X*)	TO-TA (*X*)
	TO-TA (*X*)		LO-LA (*K*,*W*)	
1*B*	LO-LA (*X*)	[d]	[e]	[d]
1*C*	LO-TA (*X*)	[d]	[e]	[d]
1*D*	[e]	[e]	[e]	[d]
1*E*	[e]	[e]	[e]	[d]
2*A*	[d]	[d]	[e]	[d]
2*B*	2 TA (*L*)	[d]	[e]	2 TA (*L*)
2*C*	2 TA (*X*)	2 TA (*X*)	2 TA (*X*)	2 TA (*X*)
2*D*	[e]	[e]	[e]	[d]
3	LO-TA (*X*)	TA+LA (*X*)	2 TA (*W*)	TA+LA (*X*)
4	2 LA (*X*)	2 LA (*X*)	2 LA (*W*)	2 A_2(*W*)
5	2 LA (*X*)	2 LA (*X*)	2 LA (*K*)	2 LA (*X*)
6	TA+TO (*X*)	TA+TO (*X*)	TA+TO (*X*)	TA+TO (*X*)
7	LA+TO (*X*)	TA+LO (*L*)	TA+TO (*W*)	LA+TO (*X*)
		LA+TO (*X*)	LA+LO (*W*)	
8*A*	TA+LO (*X*)	TA+LO (*L*,*X*)	LA+LO (*K*)	TA+LO (*L*)
8*B*	[e]	[d]	[e]	LA+LO (*X*)
8*C*	[e]	[d]	[e]	[d]
9	[e]	2 TO (*X*)	2 TO (*X*)	e
10	TO+LO (*L*,*X*,Γ)	TO+LO (*L*,*X*)	2 TO (*W*)	TO+LO (*L*,*X*,Γ)
			2 LO (*K*,*W*)	
11*A*	2 LO (*X*)	2 LO (*X*)	[e]	2 LO (*X*)
11*B*	2 LO (*L*)	2 LO (*L*)	[e]	2 LO (*L*)
11*C*	2 LO (Γ)	[e]	[e]	2 LO (Γ)
12	[e]	2ν (H^-)	[e]	2ν (H^-)

[a]Reference 7.
[b]Reference 9.
[c]Reference 10.
[d]Not assigned.
[e]Not observed.

previously been made on the basis of measurements made only at ambient pressure. A summary of the self-consistent pressure dependence checks that we have done is shown in Table II.

It has turned out that the assignments of features involving the *X* point are more straightforward than it is elsewhere in the Brillouin zone. This is because all phonon combinations at the *X* point are allowed by the selection rules for second-order Raman scattering in the rocksalt structure.[28]

In Fig. 7(a) we show that the frequency of feature 3 [TA+LA (*X*)] is the average of features 2*C* [2TA (*X*)] and 5 [2LA (*X*)] for LiD. The same relation holds for LiH. This

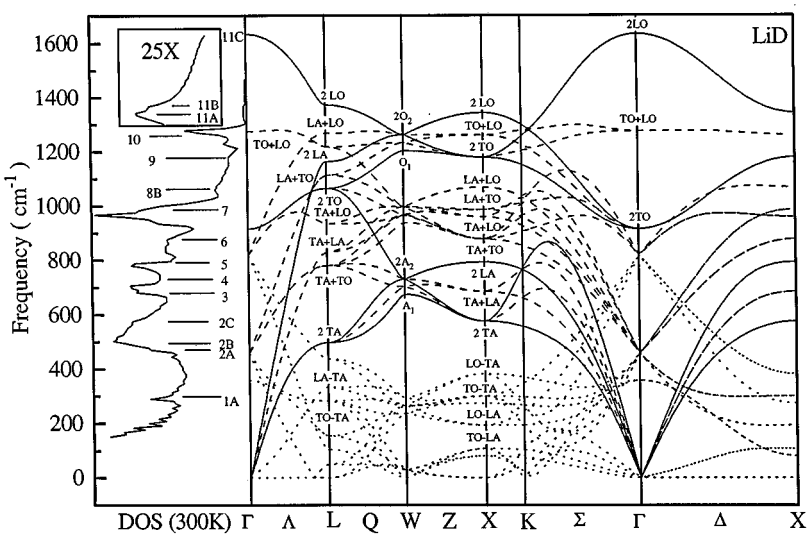

FIG. 6. The two-phonon dispersion curves and the two-phonon density of states of LiD calculated using the shell-model fit to the neutron-scattering data (Ref. 6). The dispersion curves for the overtone modes, combination modes, and difference modes are shown as the solid, dashed, and dotted lines, respectively.

TABLE II. Assignment checks between observed features. We have compared various combinations of the frequencies of features as a function of pressure in an attempt to check for the internal consistency of assignments that have been proposed. The first column gives the primary feature and its tentative assignment. The second column gives the equation which was used to obtain an equivalent expression along with their assignment. The third column gives the panel of Fig. 7 where this comparison is presented. The last two columns show the results of the check for both LiH and LiD ($\surd$ = agreement, X = disagreement).

Assignment checked	Comparison made	Figures	LiH	LiD
	Optic minus acoustic difference modes			
$1A$ TO-LA (X)	$\nu_6-\nu_{2C}/2-\nu_5/2$ [TA+TO]−[2TA]/2−[2LA]/2	9	X	X
$1A$ TO-TA (X)	$\nu_6-\nu_{2C}$ [TA+TO]−[2TA]	9	$\surd$	$\surd$
$1B$ LO-LA (X)	$(\nu_{11A}-\nu_5)/2$ ([2LO]−[2LA])/2	9	X	X
$1C$ LO-TA (X)	$(\nu_{11A}-\nu_{2C})/2$ ([2LO]−[2TA])/2	9	X	X
	Acoustic sum mode			
$2C$,3,5 TA+LA (X)	$(\nu_{2C}+\nu_5)/2$ ([2TA]+[2LA])/2	7(a)	$\surd$	$\surd$
	Acoustic plus optic sum modes			
6 TA+TO (X)	$\nu_{2C}/2+\nu_{10}-\nu_{11A}/2$ [2TA]/2+[TO+LO]−[2LO]/2	8	$\surd$	$\surd$
7 TA+LO (L)	$(\nu_{2B}+\nu_{11B})/2$ ([2TA]+[2LO])/2			X
7 LA+TO (X)	$\nu_5/2+\nu_{10}-\nu_{11A}/2$ [2LA]/2+[TO+LO]−[2LO]/2	8	$\surd$	$\surd$
$8A$ TA+LO (L)	$(\nu_{2B}+\nu_{11B})/2$ ([2TA]+[2LO])/2	7(d)		$\surd$
$8A$ TA+LO (X)	$(\nu_{2C}+\nu_{11A})/2$ ([2TA]+[2LO])/2	7(c)		X
$8B$ LA+LO (X)	$(\nu_5+\nu_{11A})/2$ ([2LA]+[2LO])/2	7(b)		$\surd$
	Optic sum mode			
10 TO+LO (X)	$\nu_6+\nu_{2C}/2+\nu_{11A}/2$ [TA+TO]−[2TA]/2+[2LO]/2	8	$\surd$	$\surd$

analysis fixes the frequencies of TA (X) and LA (X) in both LiH and LiD with very little uncertainty.

We now consider a few other examples of the application of the self-consistency check to the assignments of acoustic plus optic sum features. Feature $8B$ in LiD has not previously been identified. The pressure dependence of $8B$ allows us to easily assign it to LA+LO (X) as shown in Fig. 7(b). Self-consistent pressure dependence checks can also be used to reject an assignment. As shown in Fig. 7(c), feature $8A$ in LiD and the frequency of the previous assignment,[7,9] TA+LO (X) move apart as the pressure increases. We assign feature $8A$ to TA+LO (L) in accord with the pressure dependence check shown in Fig. 7(d). However, this assignment is not consistent with the selection rules for the second-order Raman scattering for rocksalt structure.[28]

For the optic modes we have less data than we do for the acoustic modes. Consequently, the optic phonons must be derived from both combination acoustic plus optic features as well as optic-optic sum features. We show in Fig. 8 determinations of the TO (X) and LO (X) in both LiD and LiH by several methods. The frequency axis for LiH is scaled with the $\sqrt{2}$ factor with respect that for LiD. The pressure dependence of LO (X) in LiD is very well determined from the overtone feature $11A$ [2LO (X)]. We demonstrate several ways of obtaining TO (X). We can calculate TO (X), ■, in LiD from features $2C$ [2TA (X)] and 6 [TA+TO (X)] because we have the pressure-dependent frequency for feature 6 over the entire pressure range. This determination will be used for the further analysis. We can also use feature 5 [2LA (X)] and feature 7 [LA+TO (X)], ◆. This is in fair agreement with the TO (X) determined from features $2C$ and 6. We also show TO (X) for LiD determined using features 10 [TO+LO (X)] and $11A$ [2LO (X)]. The pressure dependence of this determination of TO (X) does not agree as well

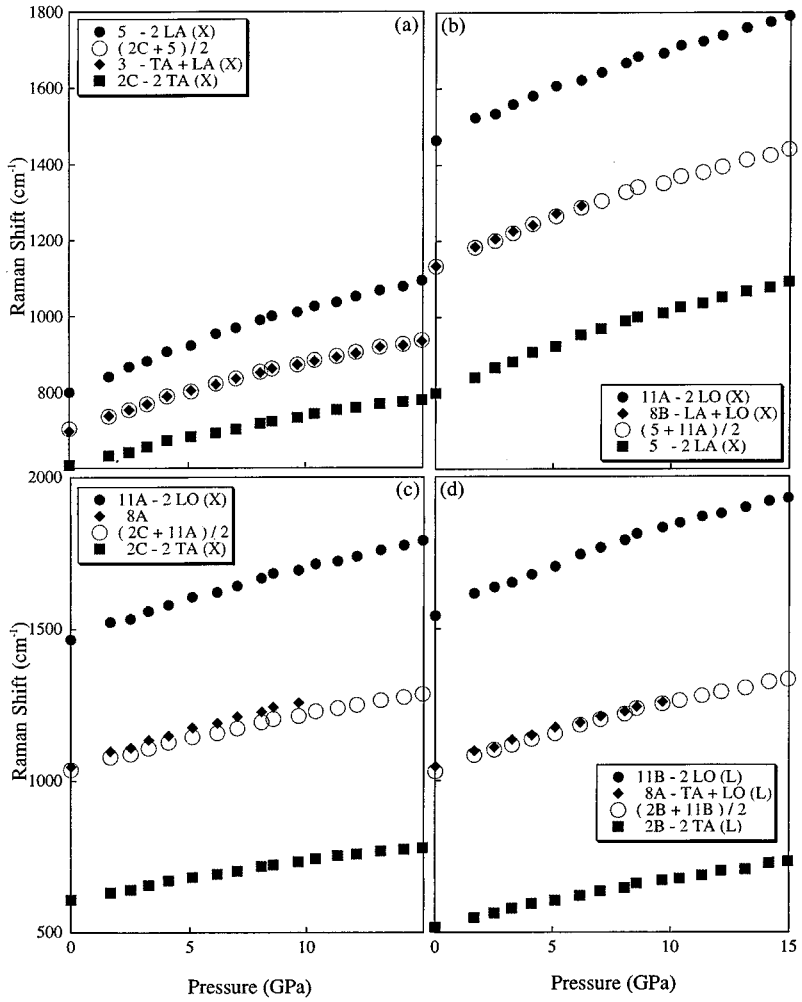

FIG. 7. Self-consistency checks between various experimental frequencies as a function of pressure. See text and Table II. (a) Comparison of acoustic sum modes in LiD. Feature $2C$ and feature 5 are used to calculate the frequency of TA+LA (X) which is compared to feature 3. (b) Comparison of LA+LO (X) with feature $8B$ in LiD. (c) Comparison of TA+LO (X) with feature $8A$ in LiD. This comparison rules out the assignment. (d) Comparison of TA+LO (L) with feature $8A$ in LiD.

at low pressure with the determinations above and therefore we do not use this TO (X) in the subsequent analysis. We attribute this to the problem mentioned before, namely that feature 10 contains contributions from many places in the Brillouin zone and therefore the pressure dependence of its center is not a reliable source of data.

In LiH we do not have data on any optic overtone features. To obtain the pressure dependence of TO (X) we used the methods as above calculating from features $2C$ [2TA (X)] and 6 [TA+TO (X)] as well as features 5 [2LA (X)] and 7 [LA+TO (X)], which is shown in Fig. 8. For the purpose of fitting, we merge the results from these two methods for determining TO (X) because the pressure ranges of data availability complement each other. We then determine an estimate of the pressure dependence of LO (X) in LiH from this TO (X) and from feature 10 since this is the only combination that includes LO (X). This determination of LO (X) in LiH is less reliable because of the problem with feature 10 mentioned before.

The assignments for the difference features are the most difficult to establish. As shown in Fig. 6, the two-phonon dispersion curves are especially dense in this region. Contributions come from the L, W, X, K points, and their neighborhoods. We have compared features $1A$, $1B$, and $1C$ in LiD with some possible assignments as suggested by the two-phonon dispersion curves in Fig. 9. It is immediately apparent that the LO-LA (X) and TO-LA (X) assignments can be ruled out because of their very different pressure dependence. The results of our comparison show that TO-TA (X) is the most likely candidate; it has by far the closest pressure dependence and it is only 10 cm^{-1} lower than feature $1A$. This result also holds true for feature $1A$ in LiH. We were not able to assign other difference features.

V. PRESSURE AND VOLUME DEPENDENCE OF PHONONS

The *pressure* dependence of the zone-boundary phonon frequencies that we have determined are nonlinear. Fits of these frequencies to second-order polynomials in pressure are given in Table III. The volume dependence of the acoustic and optic phonons are shown in Figs. 10(a) and 10(b), respectively. These plots are log-log plots of frequency vs V/V_0. The volumes are calculated from the pressure using the third-order Birch-Murnaghan EOS fit to the neutron-diffraction measurements by Besson *et al.*[19] up to 10 GPa. We have made the modest extrapolation to 15 GPa.

Mode Grüneisen parameters are typically assumed to be constant. Based upon this assumption, the mode Grüneisen parameters are obtained by fitting the phonons to an equation of the form

$$\omega_i = \omega_{0i}(V/V_0)^{-\gamma_i}. \quad (2)$$

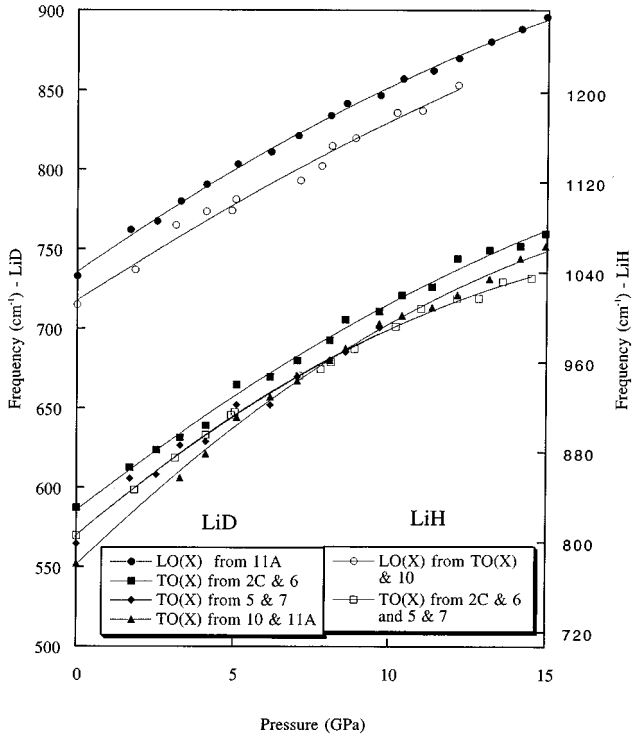

FIG. 8. LO (X) and TO (X) in LiD and LiH vs pressure. Results of various determinations. Numbers following the chart symbol inset represent the features from which determined. See text in Sec. IV C.

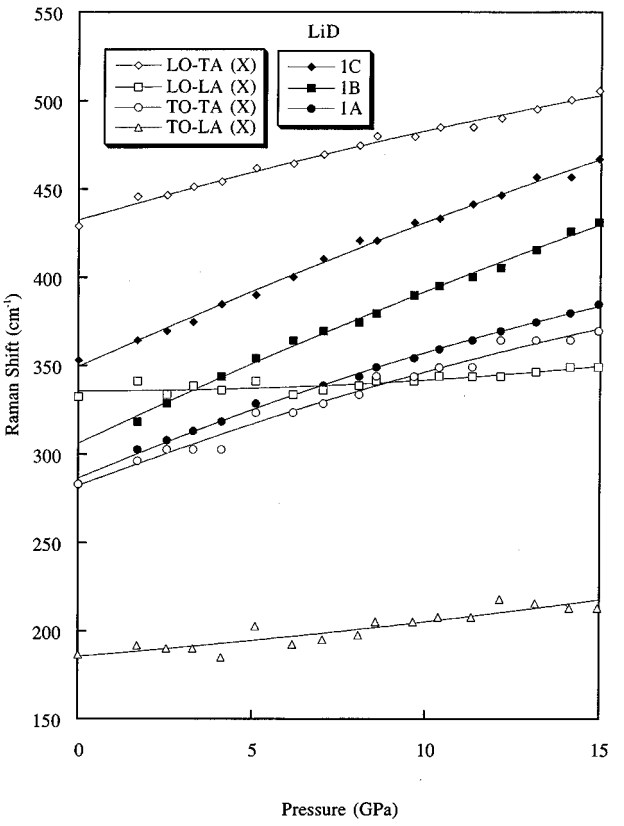

FIG. 9. Features $1A$, $1B$, and $1C$ in LiD vs pressure compared with various difference modes at X. See text in Sec. IV C.

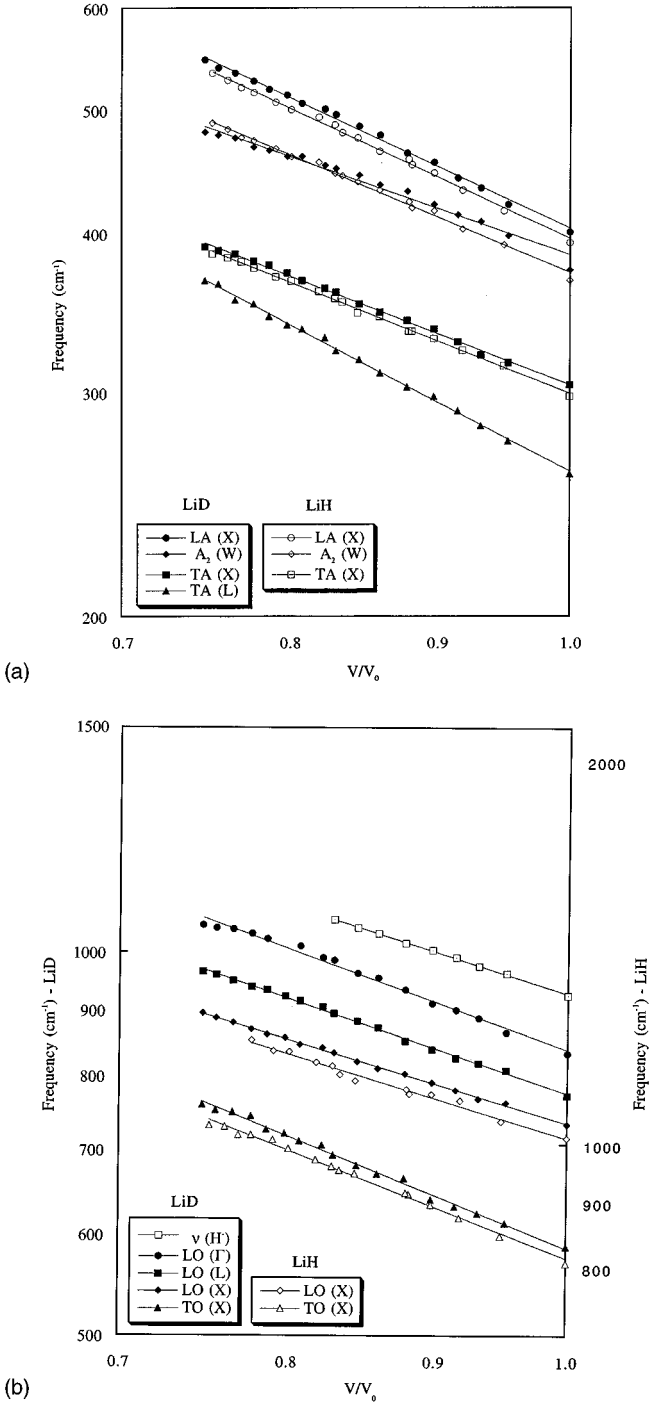

FIG. 10. The volume dependence of (a) the acoustic phonons, and (b) the optic phonons extracted from the second-order Raman spectra of LiH and LiD. The frequencies of the optic phonons in LiH are scaled by $\sqrt{2}$ relative to the LiD optic-phonon frequencies. Data are fit to a constant mode Grüneisen parameter. See Table III.

Such fits will be a straight line on a $\log\omega$ vs $\log(V/V_0)$ plot as shown in Figs. 10(a) and 10(b). The constant mode Grüneisen parameters obtained this way are given in Table III.

The straight-line fits to the data are reasonably good for the optic phonons as shown in Fig. 10(b). However, the fits to the acoustic phonons in Fig. 10(a) are less satisfactory, especially at low pressure. We have carefully remeasured the Raman spectra at ambient pressure to make certain of the

TABLE III. The pressure and volume dependence of phonons of LiH and LiD. The mode Grüneisen parameters are calculated using the EOS (Ref. 19). The phonon frequencies are derived from the overtone frequencies, except for TO (X) in LiD and TO (X) and LO (X) in LiH. TO (X) in LiD is derived from features $2C$ [2TA (X)] and 6 [TA+TO(X)]. TO (X) in LiH is deduced from features $2C$ [2TA (X)], 5 [2LA (X)], 6 [TA+TO (X)], and 7 [LA+TO (X)]. In LiH, LO (X) is determined from feature 10 [TO+LO (X)] and previously determined TO (X). The pressure and volume dependence of $A_2(W)$ and LO (Γ) in LiD must be regarded as an estimate. Values in parentheses are calculated via VIB (Ref. 20). See Figs. 10(a) and 10(b).

	$\omega_i=\omega_{0i}+a_iP+b_iP^2$						Constant mode gamma		Volume-dependent mode gamma			
	LiD			LiH			LiD	LiH	LiD		LiH	
Phonons	ω_{0i} (cm^{-1})	a_i (cm^{-1}/GPa)	b_i (cm^{-1}/GPa^2)	ω_{0i} (cm^{-1})	a_i (cm^{-1}/GPa)	b_i (cm^{-1}/GPa^2)	γ_i	γ_i	γ_{0i}	q	γ_{0i}	q
TA (L)	260±1	9.2±0.4	−0.14±0.02				1.19±0.02		1.26±0.06	0.4±0.3		
	(232)	(7.6)	(−0.11)	(220)	(8.3)	(−0.14)	(1.14)	(1.20)	(1.27)	(0.6)	(1.37)	(0.7)
TA (X)	303.2±0.8	8.2±0.2	−0.15±0.02	299.0±0.8	8.0±0.2	−0.14±0.02	0.883±0.012	0.902±0.010	0.97±0.05	0.6±0.3	0.96±0.04	0.4±0.03
	(304)	(4.7)	(−0.11)	(303)	(7.0)	(−0.16)	(0.47)	(0.65)	(0.71)	(2.6)	(0.98)	(2.4)
$A_2(W)$	378±2	11.5±0.5	−0.32±0.03	370±2	11.5±0.4	−0.24±0.03	0.80±0.03	0.96±0.02	1.29±0.05	3.1±0.3	1.15±0.05	1.2±0.3
	(399)	(10.9)	(−0.21)	(389)	(12.7)	(−0.26)	(0.86)	(0.96)	(1.14)	(1.6)	(1.27)	(1.6)
LA (X)	400.3±1.3	14.0±0.4	−0.29±0.02	393.6±1.4	13.3±0.4	−0.26±0.03	1.06±0.02	1.06±0.02	1.29±0.05	1.2±0.2	1.22±0.05	0.9±0.2
	(451)	(14.2)	(−0.24)	(443)	(15.9)	(−0.30)	(1.02)	(1.07)	(1.27)	(1.2)	(1.36)	(1.3)
TO (X)	586±3	15.6±0.8	−0.25±0.05	806±2	23.8±0.7	−0.55±0.05	0.92±0.02	0.88±0.02	0.93±0.08	0.1±0.5	1.10±0.06	1.4±0.3
	(570)	(16.6)	(−0.22)	(793)	(23.5)	(−0.36)	(1.06)	(1.01)	(1.10)	(0.2)	(1.06)	(0.3)
LO (X)	736±2	13.9±0.5	−0.23±0.03	1015±6	18±2	−0.2±0.2	0.680±0.007	0.69±0.03	0.68±0.03	0.0±0.3	0.62±0.09	−0.8±1.0
	(992)	(16.5)	(−0.21)	(1408)	(27.0)	(−0.41)	(0.67)	(0.70)	(0.63)	(−0.3)	(0.69)	(−0.1)
LO (L)	774±2	18.0±0.5	−0.34±0.03				0.77±0.01		0.84±0.04	0.6±0.3		
	(1084)	(20.5)	(−0.28)	(1569)	(31.4)	(−0.50)	(0.72)	(0.71)	(0.72)	(0.0)	(0.72)	(0.0)
LO (Γ)	829±3	24.0±0.8	−0.60±0.05				0.82±0.02		1.07±0.08	1.7±0.5		
	(1312)	(20.7)	(−0.29)	(1788)	(30.1)	(−0.48)	(0.61)	(0.61)			(0.61)	(0.0)
$\nu(H^-)$	926±2	21.1±0.9	−0.6±0.1				0.72±0.01		0.78±0.03	0.8±0.4		

data at 1 bar. This lack of straight-line behavior indicates that the mode Grüneisen parameters for these acoustic modes are not constant. It is well known that the overall Grüneisen parameter varies with density from studies in the geophysical science. Many authors[29–34] have employed a volume-dependent mode Grüneisen parameter in the form of

$$\gamma_i = \gamma_{0i}(V/V_0)^q, \tag{3}$$

where γ_{0i} is the mode Grüneisen parameter at ambient pressure and q, the second Grüneisen parameter, is the logarithmic derivative of the mode Grüneisen parameter with respect to volume. Substituting Eq. (3) into the definition of mode Grüneisen parameter, one obtains upon integrating

$$\omega_i = \omega_{0i} \exp\left\{ \frac{\gamma_{0i}}{q} [1-(V/V_0)^q] \right\}. \tag{4}$$

We have also used Eq. (4) to fit the volume dependence of all the phonon frequencies. The results of these fits are also given in Table III, however they are not shown in separate figures.

VI. DISCUSSION

The frequencies of the phonons at ambient pressure are in good agreement with the neutron-scattering data.[6] In particular, the acoustic phonons fall within 5% of that data, while the frequencies of the longitudinal optic phonons are 10% higher than the corresponding shell-model fits. This is not surprising considering no neutron-scattering data was available to fit the LO branches.

Our measurements of LO (Γ) from feature 11*C* in LiD, when extrapolated to ambient pressure as shown in Fig. 8(b), are in good agreement with the values determined by infrared reflection measurements.[8,35] This agreement gives strong support to our estimate of the location of the 2LO (Γ) feature. Several authors[10,15,22,23] have raised the conjecture that the strong uv enhanced resonance observed in the 2LO region suggests that 2LO (Γ) is the main component of both features 11*A* and 11*C*. This proposed assignment is not necessarily in disagreement with ours, however it would be very interesting to study the resonance in second-order Raman spectra at high pressure where the various 2LO features are much more separated than they are at ambient pressure.

When we compare the frequencies of the phonons vs pressure for the two iotopes, LiH and LiD we have shown that in the acoustic region the frequencies and their pressure dependence are comparable except for the case of the A_2 (W) phonon. The volume dependence of all the X point phonons for both LiH and LiD are comparable. All of these phonons scale approximately by the ratio of 1 for acoustic modes and by $\sqrt{2}$ for the optic modes shown in Figs. 10(a) and 10(b).

Substantial variations in the volume dependence between the various phonons are observed. As shown in Fig. 10(a), the volume dependence for TA (L) is greater than that for TA (X). with mode gamma's of 1.2 and 0.9, respectively. This is quite different from the rest of the acoustic phonons (see Table III). Among the optic phonons, TO (X) has the largest mode Grüneisen parameter as seen in Fig. 10(b). These results indicate that the transverse phonons have larger mode Grüneisen parameters than the longitudinal phonons. This general trend is also corroborated by our *ab initio* calculations,[20] with the exception of TA (X) and LA (X) where a large discrepancy shows up in TA (X) between experiment and theory.

We can compare the acoustic mode Grüneisen parameters with the mode Grüneisen parameters determined by ultrasonic measurements[36] on LiH. We compare the zone-edge values determined in LiD and assume that the values for LiH would be essentially the same. The mode Grüneisen parameters determined by ultrasonic measurements are very anisotropic with values ranging from 0.5 to 2.15. Along the Δ direction (00ζ), γ_{TA} at the zone center is 0.5, while at the zone boundary $\gamma_{\mathrm{TA}}(X)$ is 0.9; $\gamma_{\mathrm{LA}}(\Gamma)$ at the zone center is 1.9, while at the zone boundary $\gamma_{\mathrm{LA}}(X)$ is 1.06. In the Λ direction ($\zeta\zeta\zeta$), γ_{TA} at the zone center is 1.35 while at the zone boundary $\gamma_{\mathrm{TA}}(L)$ is 1.2. This variation of the mode Grüneisen parameters with direction and especially between the zone-center and the zone-boundary phonons shows that mode Grüneisen parameters measured at the zone boundary cannot be assumed to be the same as the mode Grüneisen parameters measured at the zone center. This result is to be contrasted with recent measurements[34] of mode Grüneisen parameters for the zone-boundary phonons in MgO at high pressure which are found to be equal to the mode Grüneisen parameters determined from elastic constants.

The only other materials for which extensive studies of the pressure dependence of the zone-boundary phonons exist are the semiconductors.[2] The TA modes in these materials are characterized by negative mode Grüneisen parameters. The mode Grüneisen parameters of all the other zone-boundary phonons are comparable to our results. However, in the case of semiconductors many of the mode Grüneisen parameters cannot be determined from second-order Raman spectra and must be inferred from other studies.

In the cases where a constant mode Grüneisen parameter model is not applicable, the volume dependence of these phonons is characterized by the two Grüneisen parameters γ_0 and q. In LiD and LiH, most of the observed phonons have a q value of one or less, with the exception of A_2 (W) in LiD. A q value of less than one indicates negative curvature in the volume dependence. The volume dependence of these phonons further supports the hypothesis that the mode Grüneisen parameters decrease with increasing pressure, in agreement with previous study on the TO (Γ) in alkali halides.[37]

In the companion paper,[20] we will show that our *ab initio* calculations predict phonon frequencies that are generally in very good agreement in the acoustic region with our experimental values, and these calculations also yield mode Grüneisen parameters that are in remarkably good agreement with our results for both acoustic and optic phonons as shown in Table III. The most serious disagreement between the experimental values and the *ab initio* calculation occurs for TA (X). The theory predicts very significant difference mode gammas for the hydride and deuteride neither of which agree with our experiment. The theory paper will discuss possible reasons for the good agreement with all phonons except for the TA (X) modes.

VII. CONCLUSIONS

The nonresonant second-order Raman spectra of LiH and LiD have been measured up to 15 GPa ($\Delta V/V_0 = -0.25$) at ambient pressure. Many new features appear at high pressure. The assignments of the two-phonon features are investigated by three methods. Two methods, which have been used before, involve a comparison with the two-phonon dispersion curves derived from shell-model fits to neutron-scattering data and scaling comparisons between isotopic features. The isotope scaling approach has been greatly facilitated by the pressure-dependent data. The third method involves self-consistency checks among the various features, and has been used extensively to confirm or reject proposed assignments. Most of the two-phonon features are attributed to combinations of zone-boundary phonons at the X, L, and W points, however a few two-phonon features remain to be assigned. We have determined the pressure dependence of all of the phonons at the X point, as well as some at the L and the W points. Using the recently measured equation of state,[19] we have also determined their volume dependence and mode Grüneisen parameters. In some cases it is necessary to use a volume-dependent model with two Grüneisen parameters. These mode Grüneisen parameters are shown to be in good agreement with the results of our *ab initio* calculations. Finally, the pressure and volume dependence of the overtone of the H^- impurity mode was measured at ambient temperature.

ACKNOWLEDGMENTS

We wish to thank Professor Fritz Lüty for providing the samples. We also thank Professor José Menéndez for the use of the Laser Facility at Arizona State University. Professor John B. Page provided the shell-model codes for the computation of the two-phonon dispersion curves and the two-phonon density of states at ambient pressure and temperature. Samples were loaded using Professor George H. Wolf's diamond-anvil-cell loading facility. We also acknowledge the help we received from David P. Wright and the Materials Facility of the Goldwater Materials Science Laboratories of the Center for Solid State Science (CSSS) at Arizona State University for sample preparation. Helpful discussions with Dr. Wolfgang Windl are also appreciated. A.C.H. would like to thank the Graduate College of the Arizona State University for financial support.

*Present address: Dept. of Math. Sci. and Eng., Cornell U., Ithaca, NY

†Electronic address: Roland.Hanson@ASU.edu

[1] A. K. M. A. Islam, Phys. Status Solidi B **180**, 9 (1993).

[2] B. A. Weinstein and R. Zallen, in *Light Scattering in Solids IV*, edited by M. Cardona and G. Güntherodt (Springer-Verlag, Berlin, 1984), p. 463.

[3] A. C. Ho, Ph.D. thesis, Arizona State University, 1996.

[4] S. S. Jaswal, T. P. Sharma, and G. Wolfram, Solid State Commun. **11**, 1151 (1972).

[5] S. S. Jaswal, G. Wolfram, and T. P. Sharma, J. Phys. Chem. Solids **35**, 571 (1974).

[6] J. L. Verble, J. L. Warren, and J. L. Yarnell, Phys. Rev. **1**, 980 (1968).

[7] D. Laplaze, C. R. Acad. Sci. B **276**, 619 (1973).

[8] D. Laplaze, J. Phys. (Paris) **37**, 1051 (1976).

[9] A. Anderson and F. Lüty, Phys. Rev. B **28**, 3415 (1983).

[10] V. I. Tyutyunnik and O. I. Tyutyunnik, Phys. Status Solidi B **162**, 597 (1990).

[11] V. G. Plekhanov and V. A. Vel'tri, Sov. Phys. Solid State **33**, 1341 (1991).

[12] V. G. Plekhanov and V. A. Veltri, Solid State Commun. **83**, 531 (1992).

[13] V. G. Plekhanov, Phys. Solid State **35**, 454 (1993).

[14] V. G. Plekhanov, Opt. Spectrosc. **75**, 31 (1993).

[15] V. G. Plekhanov, Opt. Spectrosc. **76**, 59 (1994).

[16] V. G. Plekhanov, Phys. Solid State **37**, 157 (1995).

[17] V. G. Plekhanov, Opt. Spectrosc. **78**, 424 (1995).

[18] V. G. Plekhanov, Phys. Rev. B **51**, 8874 (1995).

[19] J. M. Besson, G. Weill, G. Hamel, R. J. Nelmes, J. S. Loveday, and S. Hull, Phys. Rev. B **45**, 2613 (1992).

[20] A. Chizmeshya, G. H. Wolf, A. C. Ho, and R. C. Hanson (unpublished).

[21] H. K. Mao, P. M. Bell, J. W. Shaner, and D. J. Steinberg, J. Appl. Phys. **49**, 3276 (1978).

[22] V. G. Plekhanov and A. A. O'Connel-Bronin, JETP Lett. **27**, 387 (1978).

[23] V. G. Plekhanov and V. I. Altukhov, J. Raman Spectrosc. **16**, 358 (1985).

[24] There is a slight difference in the labeling scheme between Refs. 8 and 9. Tyutyunnik and Tyutyunnik labeled their 2LO feature 12 instead of 11 since they observed two distinct features in feature 10.

[25] G. Wolfram, S. S. Jaswal, and T. P. Sharma, Phys. Rev. Lett. **29**, 160 (1972).

[26] When a vibrational mode is not purely transverse or longitudinal, only its acoustic (A) and optic (O) character is given. The subscript number labels the phonon branch in order of increasing frequency. See for example, W. Windl *et al.*, Phys. Rev. B **48**, 3164 (1993).

[27] O. Brafman and S. S. Mitra, in *Proceedings of the Second International Conference on Light Scattering in Solids*, edited by M. Balkanski (Flammarion, Paris, 1971), p. 284.

[28] E. Burstein, F. A. Johnson, and R. Loudon, Phys. Rev. **139**, A1239 (1965).

[29] H. H. Demarest, Jr., J. Phys. Chem. Solids **35**, 1393 (1974).

[30] R. Boehler, I. C. Getting, and G. C. Kennedy, J. Phys. Chem. Solids **38**, 233 (1977).

[31] R. J. Hardy and A. M. Karo, J. Phys. Chem. Solids **38**, 905 (1977).

[32] R. Boehler and J. Ramakrishnan, J. Geophys. Res. **85**, 6996 (1980).

[33] R. Boehler, J. Geophys. Res. **87**, 5501 (1982).

[34] A. Chopelas, Earth Planet. Sci. Lett. **114**, 185 (1992).

[35] M. H. Brodsky and E. Burstein, J. Phys. Chem. Solids **28**, 1655 (1967).

[36] D. Gerlich and C. S. Smith, J. Phys. Chem. Solids **35**, 1587 (1974).

[37] M. S. Shawyer and W. F. Sherman, Infrared Phys. **22**, 23 (1982).